Biomaterials 33 (2012) 7241–7250

Contents lists available at SciVerse ScienceDirect

Biomaterials

journal homepage: www.elsevier.com/locate/biomaterials

Multifunctional receptor-targeted nanocomplexes for magnetic resonance imaging and transfection of tumours

Gavin D. Kenny [a,b], Claudio Villegas-Llerena [a], Aristides D. Tagalakis [a], Frederick Campbell [c], Katharina Welser [c], Mauro Botta [d], Alethea B. Tabor [c], Helen C. Hailes [c], Mark F. Lythgoe [b], Stephen L. Hart [a,*]

[a] Molecular Immunology Unit, UCL Institute of Child Health, 30 Guilford Street, London WC1N 1EH, UK
[b] Centre for Advanced Biomedical Imaging, Department of Medicine and Institute of Child Health, University College London, London WC1E 6DD, UK
[c] Department of Chemistry, University College London, 20 Gordon Street, London WC1H 0AJ, UK
[d] Dipartimento di Scienze e Innovazione Tecnologica, Università del Piemonte Orientale "Amedeo Avogadro", Viale T. Michel 11, I-15121 Alessandria, Italy

ARTICLE INFO

Article history:
Received 2 May 2012
Accepted 22 June 2012
Available online 17 July 2012

Keywords:
Gene therapy
Liposome
MRI
Nanocomplex
Peptide

ABSTRACT

The efficient targeted delivery of nucleic acids *in vivo* provides some of the greatest challenges to the development of genetic therapies. We aim to develop nanocomplex formulations that achieve targeted transfection of neuroblastoma tumours that can be monitored simultaneously by MRI. Here, we have compared nanocomplexes comprising self-assembling mixtures of liposomes, plasmid DNA and one of three different peptide ligands derived from ApoE, neurotensin and tetanus toxin for targeted transfection *in vitro* and *in vivo*. Neurotensin-targeted nanocomplexes produced the highest levels of transfection and showed a 4.7-fold increase in transfected luciferase expression over non-targeted nanocomplexes in Neuro-2A cells. Transfection of subcutaneous Neuro-2A tumours *in vivo* with neurotensin-targeted nanocomplexes produced a 9.3-fold increase in gene expression over non-targeted controls. Confocal microscopy analysis elucidated the time course of DNA delivery with fluorescently labelled nanocomplex formulations in cells. It was confirmed that addition of a gadolinium lipid conjugate contrast agent allowed real time *in vivo* monitoring of nanocomplex localisation in tumours by MRI, which was maintained for at least 24 h. The peptide-targeted nanocomplexes developed here allow for the specific enhancement of targeted gene therapy both *in vitro* and *in vivo*, whilst allowing real time monitoring of delivery with MRI.

1. Introduction

Gene therapy has great potential for the treatment of a wide range of diseases, with one of the most studied areas being in tumour therapy. However, the introduction of genes into tumour cells *in vivo* is fraught with problems for naked plasmid DNA, such as enzymatic degradation in the circulation and non-specific, limited efficiency of cellular uptake [1]. Liposome-based nanocomplexes have been used increasingly as delivery vectors for nucleic acid delivery both *in vitro* and *in vivo* [2,3]. This rise in the use of nanocomplexes as delivery vectors is due to the protection they afford the cargo when delivered *in vivo*, their wide ranging packaging capacities from large DNA constructs to oligonucleotides, their low level of immunogenicity allowing repeated effective delivery and ease of preparation [4,5]. The versatility of the nanocomplex platform also allows the inclusion of contrast agents for detection by magnetic resonance imaging (MRI) and fluorescence microscopy to monitor biodistribution [6–9], as well as incorporation of targeting peptides to increase the specific uptake in cells of interest [10–12].

We have previously described the efficient transfection of cultured cells with a self-assembling liposome:peptide:DNA (LPD) nanocomplex formulation comprising cationic DOTMA/DOPE liposomes (L), integrin-targeting peptides (P) and plasmid DNA (D) [13,14]. Similar formulations were subsequently developed for systemic delivery of plasmid DNA to neuroblastoma tumours with novel nanocomplex formulations that demonstrated the efficacy of PEGylation and of biologically-cleavable linkers within nanocomplex formulations containing integrin-targeting peptides and PEGylated lipids [15–18]. The aim of this new study was to further develop LPD nanocomplex formulations by, i) comparing three new candidate peptide ligands in nanocomplexes to enhance the

* Corresponding author. Tel.: +44 2079052228; fax: +44 2079052810.
E-mail address: s.hart@ucl.ac.uk (S.L. Hart).

0142-9612/$ – see front matter © 2012 Elsevier Ltd. All rights reserved.
http://dx.doi.org/10.1016/j.biomaterials.2012.06.042

receptor-targeted transfection of neuroblastoma cells *in vitro* and *in vivo*, ii) by modifications of the liposome component of the LPD nanocomplex with fluorescent reagents for microscopic imaging of vector distribution at the cellular level, and iii) by modifying the liposome component with contrast agents for real time imaging of vector distribution by MRI.

The new peptide components comprised targeting ligands for the receptors ApoE [19], neurotensin [20,21] and tetanus toxin [22,23], which have been reported to be expressed on neuroblastoma cells. Each of the peptides contained, in addition to the targeting sequence, a cationic oligolysine sequence (K_{16}) to bind and condense the plasmid DNA [13]. The targeting specificity of ApoE, Nt and Tet peptides were compared in transfections in murine neuroblastoma cells and further compared and contrasted in a different cell type, human bronchial epithelial cells. Transfections with homologous nanocomplexes containing scrambled versions of the targeting sequences, which should not bind to the relevant receptors and as an additional control, the peptide K_{16}, which can condense DNA, but lacks any targeting sequence, were also prepared.

Imaging formulations were prepared by incorporating a fluorophore, rhodamine into the bilayer of the liposome component for fluorescence microscopy and a high relaxivity gadolinium chelate [24] as a MRI contrast agent. The biophysical characteristics, transfection efficiencies, targeting properties and cellular uptake of the nanocomplexes were assessed *in vitro*. Followed by *in vivo* administration by direct injection to a subcutaneous, murine neuroblastoma tumour model where gene expression and real time MRI analysis were assessed at three time points up to 24 h with targeted and non-targeted LPD nanocomplex formulations.

2. Materials and methods

2.1. Materials

The lipids (Table 1) 1,2-dioleoyl-3-trimethylammonium-propane (DOTAP), 1,2-dioleoyl-*sn*-glycero-3-phosphoethanolamine (DOPE), 1,2-dioleoyl-*sn*-glycero-3-phosphoethanolamine-*N*-(lissamine rhodamine B sulfonyl) (DOPE-Rhodamine) and 1,2-dimyristoyl-*sn*-glycero-3-phosphoethanolamine-N-diethylenetriaminepentaacetic acid (gadolinium salt) (bis(14:0 PE)-DTPA (Gd), referred to as G_A herein), were purchased from Avanti Polar Lipids Inc., (Alabaster, USA). Diethylenetriaminepentaacetic acid α,ω-bis(8-stearoylamido-3,6-dioxaoctylamide) gadolinium salt (referred to herein as G_S) was purchased from Sigma–Aldrich (Poole, UK). GdDOTA$(GAC_{12})_2$ was synthesised as described by Kielar et al. [24]. The plasmid pCI-Luc consists of the luciferase gene from pGL3 (Invitrogen, Paisley, UK) subcloned into pCI (Promega, Southampton, UK). The targeting peptides ApoE (ApoE), Neurotensin (Nt) and Tetanus (Tet), their scrambled, non-targeting equivalents (ApoES, NtS and TetS) and the control peptide K_{16} (K_{16}) (Table 2) were synthesized on a MultiSynTech Syro peptide synthesizer using Fmoc amino acids (Novabiochem, Germany) using methods previously described [15]. The K_{16} sequences were synthesised at the N-terminus of each peptide, with the exception of the Nt and NtS peptides, in which the N-terminus is blocked by the pyroglutamic acid (Pyr) residue. Details of the purification and mass spectrometry analysis of these peptides are given in the Supplementary Data.

2.2. Liposome formulation

Liposomes were formed with lipid mixtures at specific molar ratios (Table 3) to produce the following; DOTAP:DOPE (DD), DOTAP:DOPE:GdDOTA$(GAC_{12})_2$ (DDG), DOTAP:DOPE:DOPE-Rhodamine (DDR) and DOTAP:DOPE:GdDOTA$(GAC_{12})_2$:DOPE-Rhodamine (DDGR). Liposomes were prepared by dissolving the individual lipids in chloroform at 10 mg mL^{-1} and mixing them together, followed by rotary evaporation to produce a thin lipid film. Lipids were then rehydrated with sterile water whilst rotating overnight and then sonicated for an hour in a water bath to reduce the size to unilamellar liposomes [25]. The liposomes (DDG_SR) formulated from DOTAP:DOPE:diethylenetriaminepentaacetic acid α,ω-bis(8-stearoylamido-3,6-dioxaoctylamide) gadolinium salt (G_s), and (DDG_AR), formulated from DOTAP:DOPE:bis(14:0 PE)-DTPA (Gd) (G_A), were prepared at the same molar ratio to the liposome DDGR.

2.3. Liposome MRI relaxivity

DDGR, DDG_SR and DDG_AR liposomes were serially diluted in sterile water to give a range of concentrations of 1–0.06 mg mL^{-1} of the liposomes. MR imaging was performed on a 9.4T VNMRS horizontal bore (Agilent, Palo Alto, USA) using a 59/33 quadrature volume coil (Rapid, Würzburg, Germany), with 200 μL of each of the dilution series in PCR tubes placed into a Perspex holder within the RF coil. The longitudinal relaxivity, r_1, was determined from a linear fit of $1/T_1$ as a function of gadolinium (III) concentration as described previously [7].

2.4. Nanocomplex formation and characterisation

LPD nanocomplex formulations were prepared by mixing aqueous solutions of liposome (L, 1 mg mL^{-1}), peptide (P, 10 mg mL^{-1}) and plasmid DNA (D, 5 mg mL^{-1}) at a weight ratio of 1:4:1 (L:P:D), diluted to 0.01 mg mL^{-1} (DNA) in OptiMEM (Invitrogen, Paisley, UK) for *in vitro* transfections, diluted to 0.005 mg mL^{-1} (DNA) in sterile water for biophysical characterisation and diluted to 0.5 mg mL^{-1} (DNA) in sterile water for *in vivo* experiments.

The hydrodynamic size and zeta potential of the nanocomplexes were measured by dynamic light scattering (DLS) using a Malvern Nano ZS (Malvern Instruments, Malvern, UK) at a temperature of 25 °C, viscosity of 0.89 cP and a refractive index of 1.33.

2.5. Cell transfections and viability

The murine neuroblastoma cell line Neuro-2A (ATCC, Manassas, VA, USA) was maintained in Dulbecco's Modified Eagle Medium, 1% non-essential amino acids, 1 mM sodium pyruvate and 10% FCS (Invitrogen, Paisley, UK) at 37 °C in a humidified atmosphere in 5% CO_2. The human bronchial epithelial cell line 16HBE14o- was obtained from Dieter Gruenert [26] and maintained in Minimum Essential Medium Eagle's modification (Sigma–Aldrich, Poole, UK), 1% non-essential amino acids, 2 mM L-glutamine and 10% FCS (Invitrogen, Paisley, UK) at 37 °C in a humidified atmosphere with 5% CO_2.

Cells were seeded at 2×10^4 per well in 96-well plates in 175 μL of complete media and reached 60–80%. The following day when they were transfected with 25 μL of LPD nanocomplexes in OptiMEM, containing 0.25 μg of plasmid DNA, added directly to the cells in 175 μL of complete medium per well, in replicates of six. Plates were centrifuged at 1500 rpm for 5 min (400× *g*) to promote sedimentation and incubated for 24 h at 37 °C. Cells were then lysed and a chemiluminescence assay performed to measure transfected luciferase activity (Promega, Southampton, UK) and protein concentration determined using a Bio-Rad protein assay (Hemel Hempstead, UK). Luciferase activity was expressed as RLU per milligram of protein. Cell viability assays were performed with the CellTiter 96 Aqueous One Solution Cell Proliferation Assay (Promega, Southampton, UK). Luciferase, protein concentration and toxicity measurements were performed in an Optima Fluostar microplate reader (BMG Labtech, Aylesbury, UK).

2.6. Confocal microscopy

Neuro-2A cells were seeded at 2×10^5 on FluoroDishes (World Precision Instruments Inc., FL, USA) in 1.75 mL complete media. After 24 h cells were transfected with nanocomplexes in OptiMEM formulated as described above. Briefly pCI-Luc plasmid DNA labelled with Cy-5 (Kreatech, Amsterdam, Netherlands), Nt peptide and the liposome DDGR were mixed to a 1:4:1 weight ratio so that 2.5 μg DNA in 0.25 mL was added to the 1.75 mL complete media, per dish. After 5 min, 30 min and 2 h of nanocomplex transfection incubation with the cells at 37 °C in a humidified atmosphere in 5% CO_2, the cells were washed with PBS and fixed in 4% formaldehyde, permeabilised with 0.2% Triton, blocked with 1% BSA and stained for 20 min with Alexa Fluor 488 phalloidin (4U mL^{-1}, Invitrogen, Paisley, UK) and DAPI (0.1 μg mL^{-1}, Sigma–Aldrich, Poole, UK). The wells were washed and sealed in mounting media (Invitrogen, Paisley, UK) before visualising on a Carl Zeiss LSM710 laser scanning microscope system (Jena, Germany).

2.7. Animal model

Female A/J mice (Harlan Laboratories, Oxford, UK), 8–10 weeks old, were injected subcutaneously (s.c.) in the right posterior flank with 1.5×10^6 Neuro-2A cells. After 10 ± 2 days, when tumours had reached 8–12 mm in size, 100 μL of LPD nanocomplexes in 5% glucose containing 50 μg of pCI-Luc plasmid were injected intratumourally. Twenty-four hours after injection, mice were culled, and tumours, livers and kidneys were resected, frozen on liquid nitrogen and stored at −80 °C. All *in vivo* animal experiments were performed with licences issued in accordance with the United Kingdom Animals (Scientific Procedures) Act 1986 (UK).

2.8. In vivo MR imaging

MRI measurements were performed on a 9.4T VNMRS horizontal bore (Agilent, Palo Alto, USA) using a 59/33 quadrature volume coil (Rapid, Würzburg, Germany). Mice were scanned pre-administration, 4-h and 24 h post administration using a T_1 weighted fast spin echo sequence with the following parameters: TR = 700 ms; ESP = 5.02 ms; ETL = 4; Effective TE = 5.02 ms; NSA = 10; matrix = 256 × 256; FOV = 40 × 40 mm; slc = 1 mm, scan time 7 min 28 s. MR images were analysed using ImageJ software (National Institutes of Health, US), with a manually drawn region of interest (ROI) around the tumour. The signal intensity was measured and

Table 1
Structures of the lipids used to formulate the liposomes.

Lipid	Chemical name	Structure
DOPE	1,2-dioleoyl-*sn*-glycero-3-phosphoethanolamine	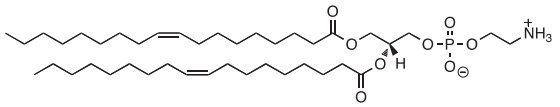
DOTAP	1,2-dioleoyl-3-trimethylammonium-propane	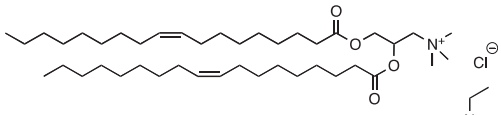
DOPE-Rhodamine	1,2-dioleoyl-*sn*-glycero-3-phosphoethanolamine-*N*-(lissamine rhodamine B sulfonyl)	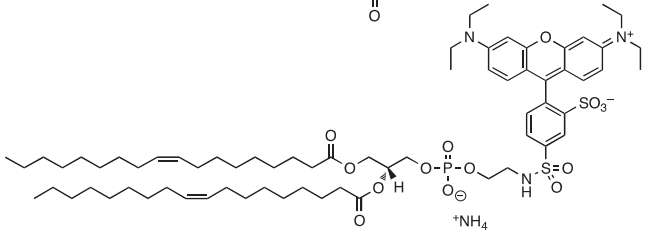
GdDOTA $(GAC_{12})_2$		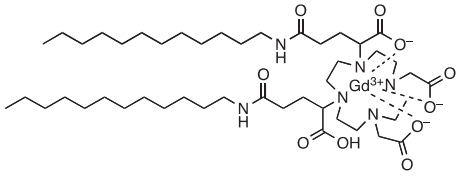
G_s	Diethylenetriaminepentaacetic acid α,ω-bis(8-stearoylamido-3,6-dioxaoctylamide) gadolinium salt	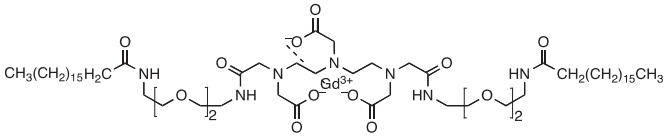
bis(14:0 PE)-DTPA (Gd) G_A	1,2-dimyristoyl-*sn*-glycero-3-phosphoethanolamine-*N*-diethylenetriaminepentaacetic acid (gadolinium salt)	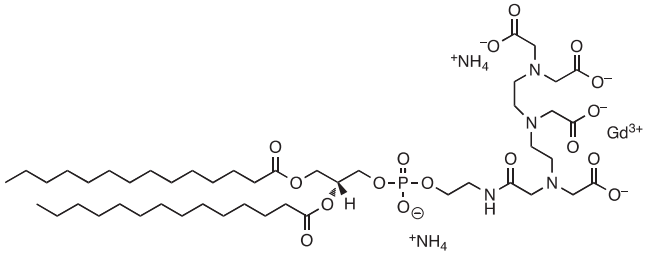

divided by the signal intensity of muscle to act as an internal reference and the percentage change in signal intensities compared. In addition the volume of each ROI was calculated and summed to give the tumour volume.

2.9. Luciferase assay on tumour and tissue extracts

Tumours, livers and kidneys were defrosted on ice, submerged in reporter gene assay lysis buffer (Roche, Basel, Switzerland), homogenized with an IKA homogenizer (IKA, Staufen, Germany), and centrifuged at 13,000 rpm (10,000 × *g*) for 10 min at 4 °C. The supernatant was removed and centrifuged at 13,000 rpm (10,000× *g*) for a further 10 min at 4 °C. Luciferase activity in the tissue lysates was measured using the Luciferase Assay System (Promega, Southampton, UK).

Table 2
Amino acid sequence and net charge of the targeted and non-targeted peptides used to formulate the LPD nanocomplexes. (Pyr = pyroglutamic acid).

Peptide	Amino acid sequence	Net charge
K16	KKKKKKKKKKKKKKKK	+16
ApoE	KKKKKKKKKKKKKKKK-GALRKLRKRLLRLRKLRKRLLRG	+28
ApoES	KKKKKKKKKKKKKKKK-GARLKLRRLKLRLKRRLKRRLLG	+28
Nt	Pyr-LYENKPRRPYILAG-KKKKKKKKKKKKKKKK	+18
NtS	Pyr-YNPKRYLIELPRAG-KKKKKKKKKKKKKKKK	+18
Tet	KKKKKKKKKKKKKKKK-GAHLNILSTLWKYRCG	+18
TetS	KKKKKKKKKKKKKKKK-GARKLSILCYWTLNHG	+18

2.10. Statistical analysis

Data presented in this study are expressed as the mean ± standard deviation and were analysed using a two-tailed, unpaired Student *t*-test where applicable.

3. Results

3.1. Liposome MRI relaxivity

The relaxivity, r_1, of the three liposomes formulated with DOTAP, DOPE, DOPE-Rhodamine and with three different lipidic gadolinium complexes, GdDOTA$(GAC_{12})_2$ (DDGR), diethylenetriaminepenta-acetic acid α,ω-bis(8-stearoylamido-3,6-dioxaoctylamide) gadolinium salt (DDG_SR) and bis(14:0 PE)-DTPA (Gd) (DDG_AR), was

Table 3
Lipid molar ratios for the liposome formulations used in the LPD nanocomplex and associated size and zeta potential, as measured by dynamic light scattering ($n = 3$, mean ± standard deviation).

Liposome	Lipid 1 (mol %)	Lipid 2 (mol %)	Lipid 3 (mol %)	Lipid 4 (mol %)	Size (nm)	Zeta (mV)
DD	DOTAP (50)	DOPE (50)			167.6 (±3.8)	46.7 (±6.7)
DDG	DOTAP (35)	DOPE (50)	GdDOTA(GAC_{12})$_2$ (15)		164.4 (±1.8)	24.5 (±1.2)
DDR	DOTAP (50)	DOPE (49)	DOPE-Rhodamine (1)		140.4 (±4.1)	+58.6 (±2.4)
DDGR	DOTAP (35)	DOPE (49)	GdDOTA(GAC_{12})$_2$ (15)	DOPE-Rhodamine (1)	163.1 (±0.4)	+2.0 (±0.1)

measured using MRI to predict the ability of the LPD nanocomplexes to act as a contrast agent for detection and monitoring *in vivo*. The relaxivity of the DDGR liposomes was calculated to equal 6.2 (±0.2) $mM^{-1}s^{-1}$, the DDG_SR liposomes was determined to be 2.8 (±0.1) $mM^{-1}s^{-1}$ and the DDG_AR liposomes to be 1.5 (±0.1) $mM^{-1}s^{-1}$ (Fig. 1). Thus DDGR appeared to be the most sensitive gadolinium-labelled liposome formulation and was used in subsequent experiments.

3.2. Biophysical characterisation of liposomes and LPD nanocomplexes

The biophysical properties of the LPD nanocomplexes were determined to provide insights into the suitability of the nanocomplexes for *in vivo* use. The parent DOTAP:DOPE (DD) liposomes were 167.6 ± 3.8 nm in diameter (Table 3). This liposome was co-formulated with peptides Nt, NtS and K_{16} and plasmid DNA to produce LPD nanocomplexes in an optimised weight ratio of 1:4:1. These nanocomplexes, ranged in size from 73.2 ± 0.9 nm for DD nanocomplexes with peptide NtS to 91.3 ± 0.6 nm with peptide Nt (Table 4). The DOTAP:DOPE:GdDOTA(GAC_{12})$_2$ (DDG) liposomes were164.4 ± 1.8 nm in diameter and their subsequent LPD nanocomplexes ranged from 89.3 ± 11.3 nm with K_{16} to 91.2 ± 3.7 nm with NtS (Table 4). DOTAP:DOPE:DOPE-Rhodamine (DDR) liposomes were 140.4 ± 4.1 nm and their nanocomplexes ranged from 79.3 ± 2.3 nm with peptide NtS to 102.3 ± 2.0 nm with peptide Nt. Finally, the liposomes formed with the DOTAP:DOPE:GdDOTA(GAC_{12})$_2$:DOPE-Rhodamine (DDGR) lipids were 163.1 ± 0.4 nm and produced the largest nanocomplexes ranging from 105.1 ± 3.6 nm with NtS to 136.8 ± 7.5 nm with K_{16}. All of the nanocomplexes formed highly cationic particles ranging from +20.2 ± 1.8 mV for $DDRK_{16}$ nanocomplexes to +68.9 ± 3.1 mV for $DDGK_{16}$ nanocomplexes (Table 4).

Overall, the DD nanocomplexes were smallest and the DDGR-containing nanocomplexes were largest regardless of the peptide co-formulated. However, there was no obvious trend in zeta potential measurements of the nanocomplexes related to the different liposome components (Table 4).

LPD nanocomplexes were also compared for the possible effects of the peptide (ApoE, neurotensin and tetanus targeting sequences, their non-targeting scrambled equivalents and the K_{16} peptide lacking a targeting sequence) on particle size and zeta potential of nanocomplexes formed with the DDGR liposome. The sizes of the nanocomplexes ranged from 105.1 ± 3.6 nm for DDGR/NtS formulations to 136.8 ± 7.5 nm for DDGR/K_{16} mixtures with no obvious trend associated with specific peptides (Table 5).

The zeta potentials ranged from +15.7 ± 7.2 mV for DDGR/TetS formulations to +49.0 ± 2.4 mV for DDGR/ApoES. ApoE and ApoES peptide nanocomplexes had the highest charges (+49.0 ± 2.4 and +42.7 ± 5.6 mV), while the tetanus peptide nanocomplexes had the lowest charge (+15.7 ± 7.2 and +27.2 ± 3.6 mV).

All of the nanocomplexes formed had a polydispersity index of less than 0.3, indicating an acceptably homogenous population of particles [27,28].

3.3. Cell transfections and viability

Assessment of cell transfection efficiency with the LPD nanocomplexes formulated with the liposome DDGR and containing different targeting peptides was performed on two cell lines, Neuro-2A and 16HBE14o-, using a luciferase gene reporter assay. The transfection efficiency of LPD nanocomplexes formed with the Nt peptide was significantly higher in the Neuro-2A cell line than with ApoE or Tet targeting peptides ($p < 0.01$). LPD nanocomplexes with Nt peptides were 1.6 fold higher than NtS, the scrambled equivalent, and 4.7-fold higher than K_{16} nanocomplexes suggesting Nt receptor-enhanced transfection. Similar transfections of the 16HBE14o- cell line showed a smaller, but significant ($p < 0.05$) enhancement by the Nt peptide when compared to the non-targeted nanocomplexes, but not to the level seen in Neuro-2A cells (Fig. 2).

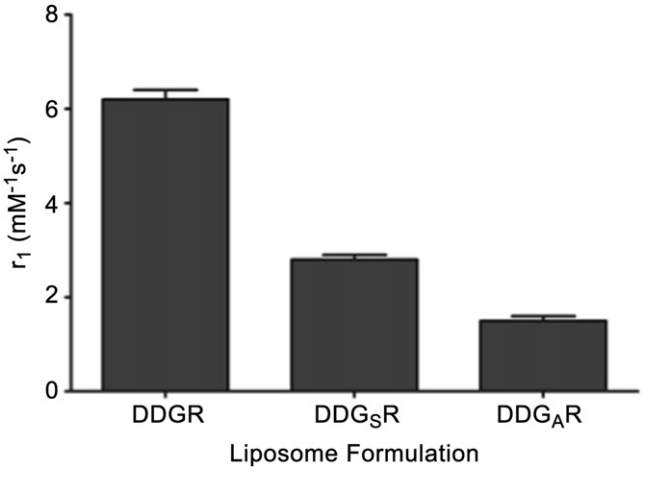

Fig. 1. Relaxivity, r_1, measurements of DDGR, DDG_SR and DDG_AR liposome formulations at 9.4T.

Table 4
Hydrodynamic size and zeta potential of LPD nanocomplexes formed at a 1:4:1 weight ratio L:P:D using DOTAP:DOPE (DD), DOTAP:DOPE:GdDOTA(GAC_{12})$_2$ (DDG), DOTAP:DOPE:DOPE-Rhodamine (DDR) and DOTAP:DOPE:GdDOTA(GAC_{12})$_2$:DOPE-Rhodamine (DDGR) liposomes, targeted and non-targeted peptides and DNA, as measured by dynamic light scattering ($n = 3$, mean ± standard deviation).

Nanocomplex	Size (nm)	Zeta potential (mV)
DD/Nt	91.3 ± 0.6	41.5 ± 1.5
DDG/Nt	90.4 ± 2.0	31.1 ± 1.0
DDR/Nt	102.3 ± 2.0	26.1 ± 2.2
DDGR/Nt	114.0 ± 1.7	35.5 ± 3.1
DD/NtS	73.2 ± 0.9	25.9 ± 2.9
DDG/NtS	91.2 ± 3.7	30.6 ± 7.6
DDR/NtS	79.3 ± 2.3	33.8 ± 2.2
DDGR/NtS	105.1 ± 3.6	25.0 ± 2.5
DD/K_{16}	78.0 ± 3.8	55.3 ± 4.8
DDG/K_{16}	89.3 ± 11.3	68.9 ± 3.1
DDR/K_{16}	98.6 ± 1.9	20.2 ± 1.8
DDGR/K_{16}	136.8 ± 7.5	35.8 ± 6.6

Table 5
Hydrodynamic size and zeta potential of LPD nanocomplexes formed at a 1:4:1 weight ratio L:P:D using the DDGR liposome, targeted and non-targeted peptides and DNA, as measured by dynamic light scattering (n = 3, mean ± standard deviation).

Nanocomplex	Size (nm)	Zeta potential (mV)
DDGR/K_{16}	136.8 ± 7.5	35.8 ± 6.6
DDGR/ApoE	119.7 ± 1.0	42.7 ± 5.6
DDGR/ApoES	117.7 ± 3.9	49.0 ± 2.4
DDGR/Nt	114.0 ± 1.7	35.5 ± 3.1
DDGR/NtS	105.1 ± 3.6	25.0 ± 2.5
DDGR/Tet	128.4 ± 5.6	27.2 ± 3.6
DDGR/TetS	115.8 ± 2.2	15.7 ± 7.2

The transfection activity of nanocomplexes formed with the ApoE targeting peptide showed a small, but significant level of enhancement compared to ApoES homologues in 16HBE14o- cells ($p < 0.05$), whereas there was no significant difference in transfection levels of these nanocomplexes in Neuro-2A cells (Fig. 2). Nanocomplexes formed with the Tet targeting peptide had higher levels of transfection than their non-targeted TetS homologues in both Neuro-2A cell (2-fold, $p < 0.01$) and in 16HBE14o- cell (5-fold, $p < 0.001$) lines, suggesting Tet peptide specificity, but interestingly, Tet LPD nanocomplexes gave lower transfection than the untargeted K_{16} nanocomplexes in both cell lines (Fig. 2).

Further cell transfections were performed to assess the effect of the four liposomes, DD, DDG, DDR and DDGR, on the transfection efficiency of LPD nanocomplex formulations with peptides Nt, NtS, and K_{16} and DNA. Nanocomplexes formulated with the unlabelled liposome DD had the highest transfection efficiency with the Nt, NtS and K_{16} peptides in Neuro-2A cells when compared to nanocomplexes containing DDG, DDR and DDGR liposomes.

The replacement of the DD liposome with DDR liposomes into the nanocomplexes with the Nt, NtS and K_{16} peptides (Fig. 3A), decreased transfection efficiency uniformly by approximately 18% for all peptide nanocomplexes. The inclusion of the gadolinium lipid into the DDG bilayer reduced transfection efficiencies by 48.3% for the Nt peptide, 65.5% for NtS and 85.6% for the K_{16} nanocomplexes. The transfection efficiency of nanocomplexes containing both the rhodamine and gadolinium lipids (DDGR) were reduced to 53.4%, 66.5% and 86.4% of the DD nanocomplexes for Nt, NtS and K_{16} nanocomplexes, respectively. However, the transfection efficiency of the targeted Nt nanocomplexes with all four liposomes remained significantly higher than each of the NtS and K_{16} nanocomplexes indicating that the substitution of liposomes did not compromise receptor-enhanced transfection (Fig. 3A). Neuro-2A cell viability, as measured by the MTS cytotoxicity assay, was greater than 80% with all of the nanocomplex formulations tested (Fig. 3B).

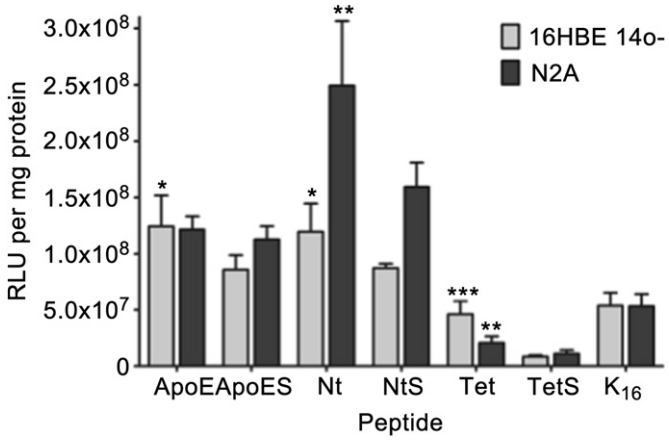

Fig. 2. Nanocomplex cell transfections in 16HBE14o- and Neuro-2A cell lines. Nanocomplexes formed with the liposome DDGR, the targeting peptides ApoE, Nt and Tet, the scrambled equivalents ApoES, NtS and TetS and the non-targeted peptide K_{16} and DNA plasmid pCI-Luc. Transfection efficiency was measured by luciferase activity and expressed as relative light units (RLU) per mg of protein with values the means of 6 replicates ± standard deviation. * = $p < 0.05$, ** = $p < 0.01$ and *** = $p < 0.001$ compared to equivalent scrambled peptide.

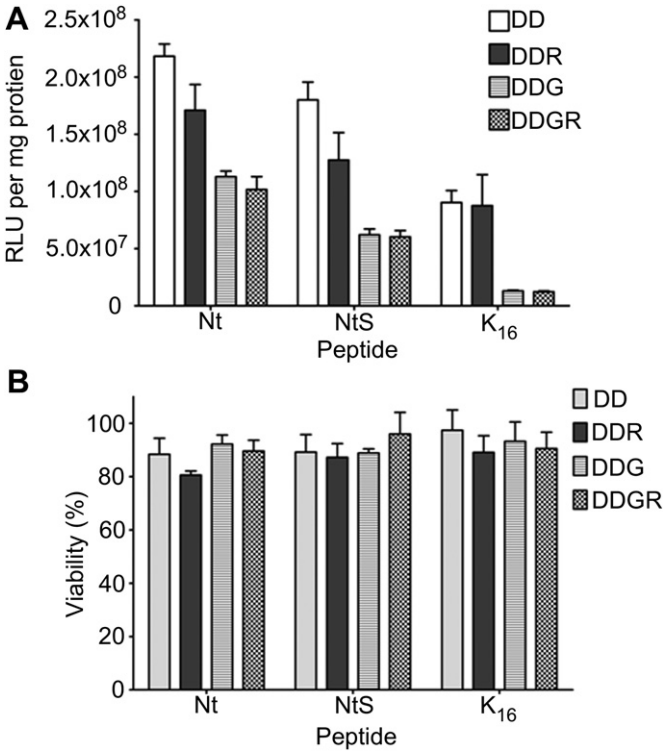

Fig. 3. Comparison of different liposomes in the nanocomplex formulation on cell transfections and viability in Neuro-2A cells. Nanocomplexes formed with the liposomes DD, DDG, DDR and DDGR, the targeting peptide neurotensin, the scrambled equivalent NtS and the non-targeted peptide K_{16} and DNA plasmid pCI-Luc. Transfection efficiency was measured by luciferase activity and expressed as relative light units (RLU) per mg of protein (A). Cell viability was measured using the MTS assay and normalised to that of untransfected cells (B). Values are the means of 6 replicates ± standard deviation.

3.4. Confocal microscopy

The early stages of uptake kinetics of the nanocomplexes in Neuro-2A cells were investigated by confocal microscopy with images taken at 5 min, 30 min and 2 h after transfection. The cells were analysed for localisation of the rhodamine-labelled lipid and the Cy-5 labelled DNA. Cells were also stained with AlexaFluor488 on F-actin in the cytoplasm and DAPI for visualisation of the nucleus. Fluorescent nanocomplexes were localised to cell membranes after 5 min incubation with none internalised. Internalisation of the nanocomplexes was visualised as early as 30 min with rhodamine and Cy-5 detected inside the cytoplasm of the cells. The intensity of rhodamine and Cy-5 inside the cell increased over time indicating progressive uptake and that internalisation of nanocomplexes was greatest after 2 h of incubation with the majority of the nanocomplexes found in perinuclear regions as suggested by the close proximity of the rhodamine and Cy-5 signals to the DAPI signal of the cell nucleus (Fig. 4).

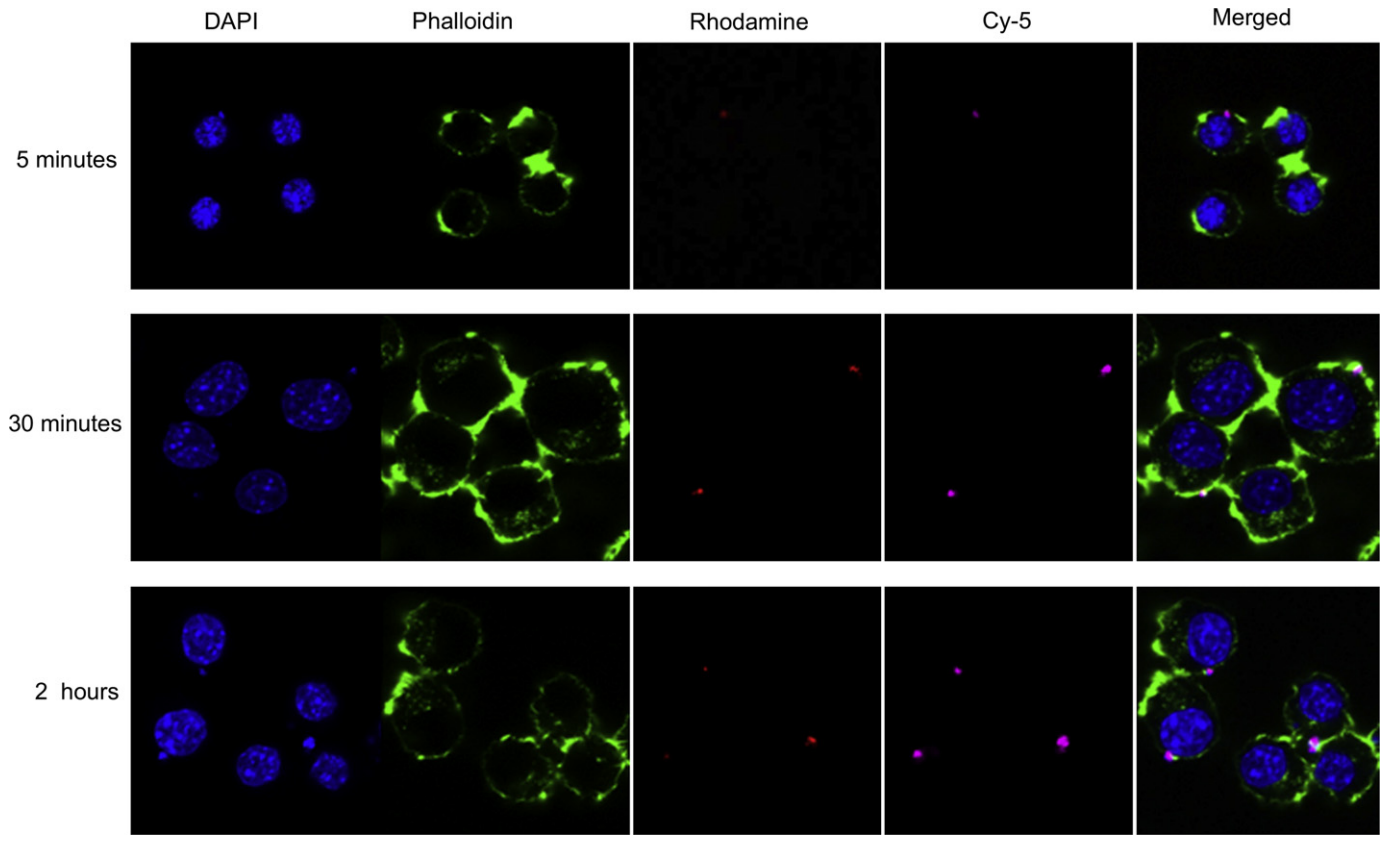

Fig. 4. Confocal microscopy of Neuro-2A cells with DDGR/Nt nanocomplexes. Cells were incubated with nanocomplexes for 5 min, 30 min or 2 h before fixing and staining for confocal microscopy. DAPI was used to visualise the nucleus of cells, Alexa Fluor 488 phalloidin to distinguish the cytoskeleton, the DOPE-Rhodamine from the lipid bilayer was used to localise the liposomes and the DNA was labelled with Cy-5.

3.5. *In vivo* MR imaging

Assessment of the ability of a gadolinium-labelled nanocomplex to act as an MR contrast agent *in vivo* was performed in a mouse tumour model. Signal intensities within the tumours were measured pre-, 4 and 24 h after injection to detect nanocomplexes containing the gadolinium-containing lipid within the liposome bilayer. Nt-targeted DDGR nanocomplexes produced a signal intensity enhancement of 21.6 ± 3.1% at 4 h and 9.1 ± 2.4% 24 h in the tumour. Administration of the K_{16} non-targeted DDGR nanocomplexes led to a signal enhancement of 16.6 ± 1.2% and 8.2 ± 1.6% at 4 and 24 h after injection respectively. These MRI signal intensities were significantly higher at both 4 h ($p < 0.01$) and 24 h ($p < 0.05$) than tumours injected with the saline control (Fig. 5A and B), but no differences were found between the targeted and non-targeted formulations. Tumour volumes, calculated from the images, increased by 43.7% between the 4 h scan and the 24 h scan.

3.6. *Luciferase assay of tumour and tissue extracts*

Luciferase gene reporter assays were performed on tumour and tissue extracts to determine the targeted transfection efficiency *in vivo*. The administration of the Nt-targeted nanocomplexes into the tumour led to a significant 9.3-fold increase ($p < 0.05$) in expression of the transfected luciferase reporter gene 24 h after injection compared to the K_{16} nanocomplexes, suggesting targeted transfection and a 160-fold increase compared to the saline control group (Fig. 5C). There were only background levels of luciferase activity in the liver and kidneys of mice injected with Nt and K_{16}-containing nanocomplexes and those injected with the saline control, with no significant differences found between samples (Fig. 5D and E).

4. Discussion

The targeted delivery of nucleic acids has great therapeutic potential for a wide range of diseases including cancers [29–33]. However, there is still need for the development of targeted synthetic nanoparticle vector formulations. Recently, the addition of contrast agents, for MRI and fluorescence microscopy, into nanocomplex formulations has shown real potential to enable monitoring of therapeutic delivery and localisation *in vivo* [7,34–36].

Previously we have demonstrated integrin-mediated targeted nanocomplex delivery of plasmid DNA to tumours *in vivo* by systemic administration [16,17]. In addition, several recent studies have also shown the potential of utilising targeting peptides (NCAM and RGD) for tumour delivery of nanocomplexes [37,38]. Here, we have investigated nanocomplexes with alternative targeting peptides to enhance tumour specificity and incorporation of MRI contrast agents and fluorophores for multimodal imaging of the nanocomplexes in transfected cells and tumours.

MRI relaxivity measurements showed that GdDOTA$(GAC_{12})_2$ lipid had the highest r_1 value when compared to DDG_SR and DDG_AR liposomes (Fig. 1). This supports previous findings that GdDOTA $(GAC_{12})_2$ is superior to the other complexes due to a more favourable water exchange rate and slower local rotation [24,39] and compares favourably to standard clinically available contrast agents, Gd-DOTA and Gd-DTPA, which have relaxivities on the order of 4 $mM^{-1}s^{-1}$ [40,41]. In addition, the macrocyclic

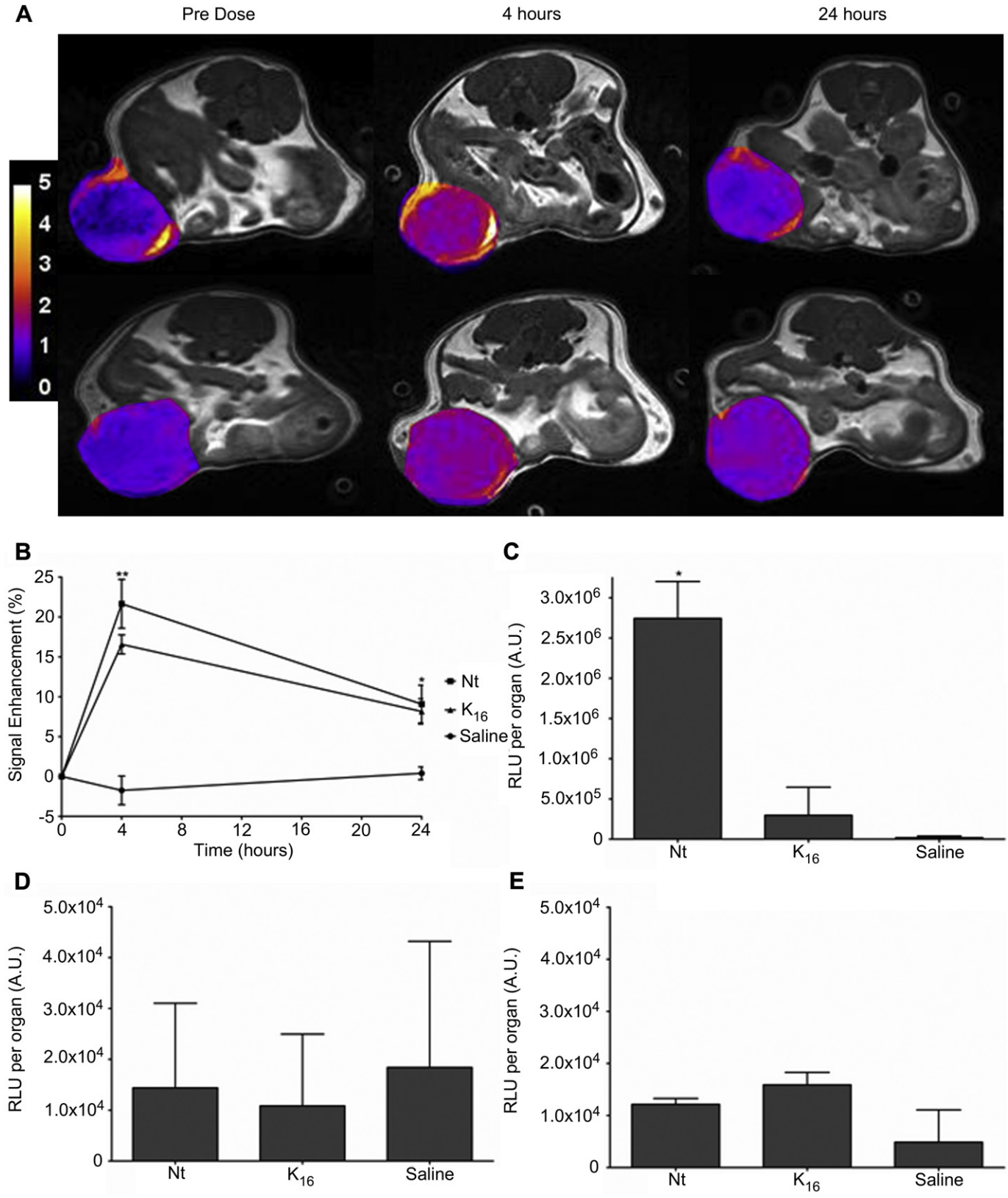

Fig. 5. *In vivo* administration of DDGR nanocomplexes. Tumours were imaged pre-, 4 and 24 h post administration of Nt-targeted (top row) and K_{16} (bottom row) DDGR nanocomplexes, producing clearly visible signal enhancements, colour scale bar units are signal intensity and arbitrary units (A). Signal intensity measurements of tumours administered with the targeting peptide Nt and non-targeted peptide K_{16} DDGR nanocomplexes produced a signal enhancement when compared to the saline control (B). Gene delivery was measured by luciferase activity at the 24 h time point and expressed as relative light units (RLU) per mg of organ, with the targeting peptide neurotensin producing a significant increase in expression over K_{16} and saline (C). Luciferase expression in the liver (D) and kidneys (E) was determined to be only background levels. $^{*} = p < 0.05$, $^{**} = p < 0.01$ compared to saline control.

gadolinium chelator, DOTA, used here is far more kinetically stable than acyclic gadolinium chelators, such as DTPA, often used in liposome formulations, as free Gd^{3+} ions decomplex from the acyclic chelators more rapidly *in vitro* and *in vivo* [42–44]. The high relaxivity and stability of liposomes containing GdDOTA$(GAC_{12})_2$ suggests they should have greater potential for *in vivo* administration than the other two liposomes.

All nanocomplexes, as expected, were monodisperse, highly cationic and with a size of around 100 nm amenable to internalization by endocytic processes [45]. The nanocomplexes were all smaller than their parent liposomes (Table 3), due to the condensing ability of the peptides (Tables 4 and 5). The DDGR nanocomplexes were largest when compared to DD, DDG and DDR, but still formed nanocomplexes of an acceptable size (Table 5). Variations in nanocomplex sizes were most likely due to differences in lipid packaging due to the larger head groups of the rhodamine and Gd-DOTA lipids in the lipid bilayer.

In vitro cell transfection studies in two different cell lines (16HBE14o- and Neuro-2A) were performed to identify the optimal targeting nanocomplexes for gene delivery using the ApoE, neurotensin (Nt) and tetanus (Tet) targeting peptides (Fig. 2). Nanocomplexes containing the Nt peptide had the highest transfection efficiency in Neuro-2A cells and expression was significantly higher than the NtS scrambled equivalent and more than four-fold higher than K_{16} nanocomplexes, suggesting that transfection was enhanced by targeting of nanocomplexes to the neurotensin receptor. The neurotensin-targeted transfection specificity for the Neuro-2A cell line is in agreement with previous studies that have shown neurotensin targets neuroblastoma tumours [46] and neurotensin nanocomplexes targeted to nigral dopamine neurons [47]. The transfection efficiency of nanocomplexes in 16HBE14o- cells with the Nt peptide was also significantly higher than with Nts scrambled control peptide and approximately 2.5-fold higher than the K_{16} control nanocomplexes, thus suggesting Nt-receptor-enhanced transfection of 16HBE14o- cells, although not to the same level as in the Neuro-2A cells. Consistent with this observation, it was reported previously that neurotensin receptors are expressed on human bronchial epithelial cells [48]. The Nt peptide, therefore offers significantly enhanced cell transfection efficiency in specific cell lines and this may be dependent on the extent of receptor expression although this requires further investigation.

Previous studies have shown uptake of nanocomplexes in endothelial cell lines using ApoE derived peptides, with the aim of crossing the blood brain barrier [49–51] and of ApoE itself for targeted delivery of siRNA to hepatic cells *in vitro* and *in vivo* [52]. Here, nanocomplexes containing the ApoE derived targeting peptide displayed a significant enhancement of transfection compared to those containing the ApoES peptide in 16HBE14o- cells. This is consistent with reports that lung epithelial cells display the low density lipoprotein receptor (LDLR) for ApoE [53]. However, although neuronal cells express receptors for ApoE [54], there was no significant difference in nanocomplex transfections of Neuro-2A cells between ApoE and ApoES peptide-containing nanocomplexes. This may reflect the fact that the ApoE peptide targeting sequence is itself highly cationic when formed as a nanocomplex, due to the twelve additional positively charged lysine and arginine residues present in the ApoE motif in addition to the sixteen lysines. This allows ApoE to bind to ubiquitous heparan sulphate proteoglycan (HSPG) receptors as well as LDLR [54]. As the ApoES peptide contains the same amino acids, but scrambled, it is also highly cationic when formed as a nanocomplex and therefore may retain the capacity to bind to HSPG despite the sequence alterations. Thus, although the experiments have shown that nanocomplexes with the ApoE targeting peptide achieved significant levels of transfection, we are unable from comparisons with the ApoES peptide to demonstrate receptor-mediated enhancement of transfection. Future studies will be required using alternative receptor-blocking agents such as antibodies or receptor cleavage reagents, as described previously [54] to clarify the receptor targeting properties of ApoE-targeted nanocomplexes in both cell lines.

Nanocomplexes containing the tetanus toxin-derived peptides (Tet) had the lowest transfection efficiency of all three targeting peptides across both cell lines, yet they displayed the highest degree of receptor-mediated specificity of transfection. Tet nanocomplexes displayed a significant enhancement of transfection in Neuro-2A cells and a highly significant five-fold enhancement in 16HBE14o- cells over nanocomplexes containing TetS. Previous data supports the evidence for tetanus-targeted specificity as nanoparticles displaying Tetanus toxin C fragment have also shown targeted transfection of neuroblastoma cells [55] and the tetanus toxin receptor is highly expressed in normal human bronchial epithelial cell lines [56,57]. The nanocomplexes containing Tet, as well as those containing TetS, both display lower transfection levels than K_{16} nanocomplexes. The zeta potential of the Tet and TetS nanocomplexes was lower than that of K_{16} DDGR nanocomplexes, which may help to partially explain this difference, although this charge difference was not reflected in size measurements. K_{16} nanocomplex formulations lack targeting ligands, but are highly cationic allowing electrostatic, binding to anionic cell surface receptors leading to non-specific-transfections in both cell lines. The Tet peptide may also have higher binding affinity for the specific receptor although this has not yet been analysed. Tet-targeted nanocomplexes may be particularly useful in applications where higher degrees of receptor-mediated specificity are required in delivery.

The addition of the rhodamine-containing and gadolinium-containing lipids into the nanocomplexes with the Nt, NtS and K_{16} peptides (Fig. 3A), decreased transfection efficiency for all nanocomplexes relative to formulations containing DOTAP/DOPE. However, despite the reduced transfection efficiency, regardless of the liposomal component, LPD nanocomplexes retained their receptor-mediated enhancement of transfection. Incorporation of rhodamine increased the nanocomplex size due presumably to the large hydrophobic rhodamine moiety. Incorporation of the gadolinium lipid had no effect on size of the DD/Nt formulation, but increased both DD/NtS and DD/K_{16}. The gadolinium-containing lipid may have had a greater effect than the rhodamine lipid on size (except for DD/Nt) and transfection efficiency when incorporated into the liposomes, as it was present in greater amounts and was accommodated at the expense of the cationic component, DOTAP (Table 3). The nanocomplexes containing both rhodamine and gadolinium lipids were correspondingly the largest formulations for each peptide class (Table 4) as might be expected, but their transfection efficiency and targeting specificity, comparing targeted to non-targeted peptide formulations (Fig. 3A) appeared to remain at acceptable levels. Cell viabilities after transfection with nanocomplexes formulated with all of the tested nanocomplexes were found to be at a suitable level for further *in vivo* studies (Fig. 3B).

Confocal microscopy analysis of Neuro-2A cells with DDGR/Nt/Cy5-labelled DNA nanocomplexes (Fig. 4), suggested that cell binding and entry occurred within the first hour and disassembly of the nanocomplexes occurred between half an hour and 2 h, in agreement with other studies published [58–61].

Since the DDGR/Nt formulation had displayed neuroblastoma cell targeted transfection *in vitro*, with transfections performed in the presence of serum, it was selected for *in vivo* experiments. Proof of principle for both targeted transfection and real time imaging of vector distribution by MRI within a subcutaneous neuroblastoma tumour was performed. To maximise the chances of detecting any difference in targeting versus non-targeting transfection *in vivo* and MRI contrast effect, the Nt peptide was compared to K_{16} peptide

and saline, injected directly into the tumour. A significant increase in signal intensity was visualised due to the presence of the nanocomplexes 4 h post administration. The decrease in signal intensity at 24 h compared to 4 h is most likely due to a combination of clearance of the nanocomplexes from the tumour and the increase in tumour size, due to growth, leading to a dilution of the gadolinium within the tumour (Fig. 5A and B). The MR signal enhancement produced by the administration of the nanocomplexes is of the same order of magnitude as other paramagnetic liposome-based tumour therapy delivery vectors [7,62]. However, further optimisation of the nanocomplex composition could increase the amount of gadolinium and hence further improve the signal enhancement. In addition, the rhodamine lipid could be utilised *ex vivo* to validate the MRI results by visualising the presence of the nanocomplexes within the tumour [7,62,63].

The targeted nanocomplexes, DDGR/Nt produced a large increase in luciferase expression when compared to the non-targeted DDGR/K_{16} nanocomplexes (Fig. 5C), despite the similar amount of nanocomplex present in the tumour as suggested by the MRI. This demonstrates that the targeting efficiency of the neurotensin-targeted nanoparticles relative to the untargeted nanocomplexes is retained *in vivo*, as previously seen in the *in vitro* experiments. Only background levels of luciferase activity were detected in the liver and kidneys (Fig. 5D and E), which suggests that there was minimal shedding of nanocomplexes from the tumour into the circulation, an essential feature for any potential clinically translatable methodology.

The targeted specificity of transfection contrasted strongly with the MRI data, which revealed no contrast enhancement with the Nt-targeted relative to the untargeted K_{16} formulation. This suggests that the MRI contrast was produced by accumulation of the nanocomplex-associated gadolinium chelate within the tumour, but was not influenced by cell uptake. Whereas transfected luciferase gene expression requires cell uptake, nuclear transport, transcription and translation. Transfection, in contrast to MRI, appears to be a highly receptor-dependent process, due most likely to improved cell binding and internalisation of the nanocomplex, increasing the amount of internalised DNA per cell.

In vivo transfections were performed in this study by direct, intratumoural administration rather than by systemic administration, as we have reported previously [16,17]. This approach was adopted to maximise delivery of the nanocomplexes to the tumour to assess the concept that gadolinium-labelling of nanocomplexes enables them to be detected *in vivo* and to evaluate the tumour targeting properties of the Nt peptide within the nanocomplex formulation *in vivo*. This study has shown that real time imaging by MRI can be used to track the distribution and persistence of a gadolinium-labelled nanocomplex *in vivo*, but not necessarily the nanocomplexes functionality. This could be assessed in future studies by analysis of tumours by luminescence and fluorescence imaging systems to monitor luciferase and GFP reporter gene expression for comparison with MRI data. The tools developed in this study will now enable such studies to be performed.

5. Conclusions

This study describes the development LPD nanocomplexes for targeted tumour cell transfection and for monitoring of vector distribution in real time by MRI. In addition fluorescence labelling was incorporated for post transfection cellular analysis of vector distribution. LPD nanocomplexes formulated with three different targeting peptides, ApoE, neurotensin and tetanus, displayed targeted transfection in both bronchial epithelial and neuroblastoma cell lines *in vitro*. Neurotensin nanocomplexes demonstrated targeted transfection in an *in vivo* neuroblastoma tumour model. These highly versatile nanocomplexes have real potential as research tools in the future development of nucleic acid therapies for cancers.

Acknowledgements

This work was funded by the Engineering and Physical Sciences Research Council (EPSRC; EP/G061521/1). The British Heart Foundation funded ML for the MRI scanner. We would like to thank the Department of Biochemical Engineering, UCL for use of their Malvern Nano ZS and also thanks to Dr Bertrand Vernay from the Institute of Child Health UCL for his advice on the confocal microscopy experiments.

Appendix A. Supplementary material

Supplementary data associated with this article can be found, in the online version, at http://dx.doi.org/10.1016/j.biomaterials.2012.06.042.

References

[1] Kawabata K, Takakura Y, Hashida M. The fate of plasmid DNA after intravenous injection in mice: involvement of scavenger receptors in its hepatic uptake. Pharmaceut Res 1995;12:825–30.
[2] Fenske DB, Chonn A, Cullis PR. Liposomal nanomedicines: an emerging field. Toxicol Pathol 2008;36:21–9.
[3] El Aneed A. An overview of current delivery systems in cancer gene therapy. J Control Release 2004;94:1–14.
[4] Gabizon AA, Shmeeda H, Zalipsky S. Pros and cons of the liposome platform in cancer drug targeting. J Liposome Res 2006;16:175–83.
[5] Kawakami S, Hashida M. Targeted delivery systems of small interfering RNA by systemic administration. Drug Metab Pharmacokinet 2007;22:142–51.
[6] Kamaly N, Kalber T, Kenny G, Bell J, Jorgensen M, Miller A. A novel bimodal lipidic contrast agent for cellular labelling and tumour MRI. Org Biomol Chem 2010;8:201–11.
[7] Kenny GD, Kamaly N, Kalber TL, Brody LP, Sahuri M, Shamsaei E, et al. Novel multifunctional nanoparticle mediates siRNA tumour delivery, visualisation and therapeutic tumour reduction in vivo. J Control Release 2011;149:111–6.
[8] Mulder WJ, Strijkers GJ, van Tilborg GA, Griffioen AW, Nicolay K. Lipid-based nanoparticles for contrast-enhanced MRI and molecular imaging. NMR Biomed 2006;19:142–64.
[9] Erdogan S, Medarova ZO, Roby A, Moore A, Torchilin VP. Enhanced tumor MR imaging with gadolinium-loaded polychelating polymer-containing tumor-targeted liposomes. J Magn Reson Imaging 2008;27:574–80.
[10] Song S, Liu D, Peng J, Sun Y, Li Z, Gu JR, et al. Peptide ligand-mediated liposome distribution and targeting to EGFR expressing tumor in vivo. Int J Pharm 2008.
[11] Chen Y, Wu JJ, Huang L. Nanoparticles targeted with NGR motif deliver c-myc siRNA and doxorubicin for anticancer therapy. Mol Ther 2010;18:828–34.
[12] Ko YT, Falcao C, Torchilin VP. Cationic liposomes loaded with pro-apoptotic peptide D-$(KLAKLAK)_2$ and bcl-2 antisense oligodeoxynucleotide G3139 for enhanced anticancer therapy. Mol Pharm 2009;6:971–7.
[13] Hart SL, Arancibia-Carcamo CV, Wolfert MA, Mailhos C, O'Reilly NJ, Ali RR, et al. Lipid-mediated enhancement of transfection by a nonviral integrin-targeting vector. Hum Gene Ther 1998;9:575–85.
[14] Siapati KE, Barker S, Kinnon C, Michalski A, Anderson R, Brickell P, et al. Improved antitumour immunity in murine neuroblastoma using a combination of IL-2 and IL-12. Br J Cancer 2003;88:1641–8.
[15] Mustapa MFM, Grosse SM, Kudsiova L, Elbs M, Raiber E-A, Wong JB, et al. Stabilized integrin-targeting ternary LPD (lipopolyplex) vectors for gene delivery designed to disassemble within the target cell. Bioconjug Chem 2009;20:518–32.
[16] Grosse SM, Tagalakis AD, Mustapa MFM, Elbs M, Meng Q-H, Mohammadi A, et al. Tumor-specific gene transfer with receptor-mediated nanocomplexes modified by polyethylene glycol shielding and endosomally cleavable lipid and peptide linkers. FASEB J 2010;24:2301–13.
[17] Tagalakis AD, Grosse SM, Meng Q-H, Mustapa MFM, Kwok A, Salehi SE, et al. Integrin-targeted nanocomplexes for tumour specific delivery and therapy by systemic administration. Biomaterials 2011;32:1370–6.
[18] Wong JB, Grosse S, Tabor AB, Hart SL, Hailes HC. Acid cleavable PEG-lipids for applications in a ternary gene delivery vector. Mol BioSyst 2008;4:532–41.
[19] Mousazadeh M, Palizban A, Salehi R, Salehi M. Gene delivery to brain cells with apoprotein E derived peptide conjugated to polylysine (apoEdp-PLL). J Drug Target 2007;15:226–30.
[20] Tyler BM, Douglas CL, Fauq A, Pang Y-P, Stewart JA, Cusack B, et al. In vitro binding and CNS effects of novel neurotensin agonists that cross the blood–brain barrier. Neuropharmacology 1999;38:1027–34.

[21] Martinez-Fong D, Navarro-Quiroga I, Ochoa I, Alvarez-Maya I, Meraz MA, Luna J, et al. Neurotensin-SPDP-poly-l-lysine conjugate: a nonviral vector for targeted gene delivery to neural cells. Mol Brain Res 1999;69: 249–62.
[22] Liu JK, Teng Q, Garrity-Moses M, Federici T, Tanase D, Imperiale MJ, et al. A novel peptide defined through phage display for therapeutic protein and vector neuronal targeting. Neurobiol Dis 2005;19:407–18.
[23] Park I-K, Lasiene J, Chou S-H, Horner PJ, Pun SH. Neuron-specific delivery of nucleic acids mediated by Tet1-modified poly(ethylenimine). J Gene Med 2007;9:691–702.
[24] Kielar F, Tei L, Terreno E, Botta M. Large relaxivity enhancement of paramagnetic lipid nanoparticles by restricting the local motions of the Gd^{III} chelates. J Am Chem Soc 2010;132:7836–7.
[25] Baraldo K, Leforestier N, Bureau M, Mignet N, Scherman D. Sphingosine-based liposome as DNA vector for intramuscular gene delivery. Pharmaceut Res 2002;19:1144–9.
[26] Cozens AL, Yezzi MJ, Kunzelmann K, Ohrui T, Chin L, Eng K, et al. CFTR expression and chloride secretion in polarized immortal human bronchial epithelial cells. Am J Resp Cell Mol 1994;10:38–47.
[27] Ma P, Dong X, Swadley CL, Gupte A, Leggas M, Ledebur HC, et al. Development of idarubicin and doxorubicin solid lipid nanoparticles to overcome Pgp-mediated multiple drug resistance in leukemia. J Biomed Nano 2009;5: 151–61.
[28] Kim J-Y, Kim J-K, Park J-S, Byun Y, Kim C-K. The use of PEGylated liposomes to prolong circulation lifetimes of tissue plasminogen activator. Biomaterials 2009;30:5751–6.
[29] Davis ME, Chen Z, Shin DM. Nanoparticle therapeutics: an emerging treatment modality for cancer. Nat Rev Drug Discov 2008;7:771–82.
[30] Bainbridge JWB, Smith AJ, Barker SS, Robbie S, Henderson R, Balaggan K, et al. Effect of gene therapy on visual function in leber's congenital amaurosis. New Engl J Med 2008;358:2231–9.
[31] Cartier N, Hacein-Bey-Abina S, Bartholomae CC, Veres G, Schmidt M, Kutschera I, et al. Hematopoietic stem cell gene therapy with a lentiviral vector in X-linked adrenoleukodystrophy. Science 2009;326:818–23.
[32] Morgan RA, Dudley ME, Wunderlich JR, Hughes MS, Yang JC, Sherry RM, et al. Cancer regression in patients after transfer of genetically engineered lymphocytes. Science 2006;314:126–9.
[33] Ott MG, Schmidt M, Schwarzwaelder K, Stein S, Siler U, Koehl U, et al. Correction of X-linked chronic granulomatous disease by gene therapy, augmented by insertional activation of MDS1-EVI1, PRDM16 or SETBP1. Nat Med 2006;12:401–9.
[34] Sumer B, Gao J. Theranostic nanomedicine for cancer. Nanomedicine 2008;3: 137–40.
[35] Bartlett DW, Su H, Hildebrandt IJ, Weber WA, Davis ME. Impact of tumor-specific targeting on the biodistribution and efficacy of siRNA nanoparticles measured by multimodality in vivo imaging. Proc Natl Acad Sci U S A 2007; 104:15549–54.
[36] Mikhaylova M, Stasinopoulos I, Kato Y, Artemov D, Bhujwalla ZM. Imaging of cationic multifunctional liposome-mediated delivery of COX-2 siRNA. Cancer Gene Ther 2009;16:217–26.
[37] Grange C, Geninatti-Crich S, Esposito G, Alberti D, Tei L, Bussolati B, et al. Combined delivery and magnetic resonance imaging of neural cell adhesion molecule-targeted doxorubicin-containing liposomes in experimentally induced kaposi's sarcoma. Cancer Res 2010;70:2180–90.
[38] Li W, Su B, Meng S, Ju L, Yan L, Ding Y, et al. RGD-targeted paramagnetic liposomes for early detection of tumor: in vitro and in vivo studies. Eur J Radiol 2011;80:598–606.
[39] Bertini I, Bianchini F, Calorini L, Colagrande S, Fragai M, Franchi A, et al. Persistent contrast enhancement by sterically stabilized paramagnetic liposomes in murine melanoma. Magn Reson Med 2004;52:669–72.
[40] Nieminen MT, Rieppo J, Silvennoinen J, Töyräs J, Hakumäki JM, Hyttinen MM, et al. Spatial assessment of articular cartilage proteoglycans with Gd-DTPA-enhanced T1 imaging. Magn Reson Med 2002;48:640–8.
[41] de Sousa PL, Livramento JB, Helm L, Merbach AE, Même W, Doan B-T, et al. In vivo MRI assessment of a novel Gd^{III}-based contrast agent designed for high magnetic field applications. Contrast Media Mol Imag 2008;3:78–85.
[42] Overoye-Chan K, Koerner S, Looby RJ, Kolodziej AF, Zech SG, Deng Q, et al. EP-2104R: a fibrin-specific gadolinium-based MRI contrast agent for detection of thrombus. J Am Chem Soc 2008;130:6025–39.
[43] Unger EC, Fritz TA, Tilcock C, New TE. Clearance of liposomal gadolinium: in vivo decomplexation. J Magn Reson Imaging 1991;1:689–93.
[44] Mier W, Hoffend J, Kramer S, Schuhmacher J, Hull WE, Eisenhut M, et al. Conjugation of DOTA using isolated phenolic active esters: the labeling and biodistribution of albumin as blood pool marker. Bioconjug Chem 2005;16: 237–40.
[45] Gao H, Shi W, Freund LB. Mechanics of receptor-mediated endocytosis. Proc Natl Acad Sci U S A 2005;102:9469–74.
[46] Rubio-Zapata HA, Rembao-Bojorquez JD, Arango-Rodriguez ML, Dupouy S, Forgez P, Martinez-Fong D. NT-polyplex: a new tool for therapeutic gene delivery to neuroblastoma tumors. Cancer Gene Ther 2009;16:573–84.
[47] Gonzalez-Barrios JA, Lindahl M, Bannon MJ, Anaya-Martinez V, Flores G, Navarro-Quiroga I, et al. Neurotensin polyplex as an efficient carrier for delivering the human GDNF gene into nigral dopamine neurons of hemiparkinsonian rats. Mol Ther 2006;14:857–65.
[48] Frankel A, Tsao M-S, Viallet J. Receptor subtype expression and responsiveness to bombesin in cultured human bronchial epithelial cells. Cancer Res 1994;54:1613–6.
[49] Sauer I, Dunay IR, Weisgraber K, Bienert M, Dathe M. An apolipoprotein E-derived peptide mediates uptake of sterically stabilized liposomes into brain capillary endothelial cells. Biochemistry 2005;44:2021–9.
[50] Re F, Cambianica I, Zona C, Sesana S, Gregori M, Rigolio R, et al. Functionalization of liposomes with ApoE-derived peptides at different density affects cellular uptake and drug transport across a blood-brain barrier model. Nanomedicine 2011;7:551–9.
[51] Re F, Cambianica I, Sesana S, Salvati E, Cagnotto A, Salmona M, et al. Functionalization with ApoE-derived peptides enhances the interaction with brain capillary endothelial cells of nanoliposomes binding amyloid-beta peptide. J Biotechnol 2011;156:341–6.
[52] Akinc A, Querbes W, De S, Qin J, Frank-Kamenetsky M, Jayaprakash KN, et al. Targeted delivery of RNAi therapeutics with endogenous and exogenous ligand-based mechanisms. Mol Ther 2010;18:1357–64.
[53] Yao X, Vitek MP, Remaley AT, Levine SJ. Apolipoprotein mimetic peptides: a new approach for the treatment of asthma. Front Pharmacol 2012;3.
[54] Michikawa M, Fan Q-W, Isobe I, Yanagisawa K. Apolipoprotein E exhibits isoform-specific promotion of lipid efflux from astrocytes and neurons in culture. J Neurochem 2000;74:1008–16.
[55] Townsend SA, Evrony GD, Gu FX, Schulz MP, Brown Jr RH, Langer R. Tetanus toxin C fragment-conjugated nanoparticles for targeted drug delivery to neurons. Biomaterials 2007;28:5176–84.
[56] Yoshida S, Fukumoto S, Kawaguchi H, Sato S, Ueda R, Furukawa K. Ganglioside GD2 in small cell lung cancer cell lines. Cancer Res 2001;61:4244–52.
[57] Galli T, Zahraoui A, Vaidyanathan VV, Raposo G, Tian JM, Karin M, et al. A novel tetanus neurotoxin-insensitive vesicle-associated membrane protein in SNARE complexes of the apical plasma membrane of epithelial cells. Mol Biol Cell 1998;9:1437–48.
[58] Bellavance M-A, Poirier M-B, Fortin D. Uptake and intracellular release kinetics of liposome formulations in glioma cells. Int J Pharm 2010;395:251–9.
[59] Elouahabi A, Ruysschaert J-M. Formation and intracellular trafficking of lipoplexes and polyplexes. Mol Ther 2005;11:336–47.
[60] Billiet L, Gomez J-P, Berchel M, Jaffrès P-A, Le Gall T, Montier T, et al. Gene transfer by chemical vectors, and endocytosis routes of polyplexes, lipoplexes and lipopolyplexes in a myoblast cell line. Biomaterials 2012;33:2980–90.
[61] Gopal V, Xavier J, Dar GH, Jafurulla M, Chattopadhyay A, Rao NM. Targeted liposomes to deliver DNA to cells expressing 5-HT receptors. Int J Pharm 2011;419:347–54.
[62] Kluza E, Jacobs I, Hectors SJCG, Mayo KH, Griffioen AW, Strijkers GJ, et al. Dual-targeting of $\alpha v\beta 3$ and galectin-1 improves the specificity of paramagnetic/fluorescent liposomes to tumor endothelium in vivo. J Control Release 2012; 158:207–14.
[63] Kamaly N, Kalber T, Ahmad A, Oliver MH, So P-W, Herlihy AH, et al. Bimodal paramagnetic and fluorescent liposomes for cellular and tumor magnetic resonance imaging. Bioconjug Chem 2008;19:118–29.